#### FULL LENGTH ARTICLE



Check for updates



# Effect of captivity on the vertebral bone microstructure of xenarthran mammals

Ellianna H. Zack 🗅 | Stephanie M. Smith | Kenneth D. Angielczyk |

Negaunee Integrative Research Center, Field Museum of Natural History, Chicago, Illinois, USA

#### Correspondence

Ellianna H. Zack, Negaunee Integrative Research Center, Field Museum of Natural History, 1400 S. Lake Shore Drive, Chicago, IL 60605, USA. Email: elliannazack@gmail.com

### **Funding information**

Anat Rec. 2021:1-18.

Field Museum of Natural History; Women in Science Postdoctoral Fellowship; National Science Foundation, Grant/ Award Number: DBI 1811627; University of Chicago Biological Sciences Collegiate Division Ecology and Evolution Fellowship; University of Chicago Careers in STEM Summer Research Grant

#### **Abstract**

Captive specimens in museum collections facilitate study of rare taxa, but the lifestyles, diets, and lifespans of captive animals differ from their wild counterparts. Trabecular bone architecture adapts to in vivo forces, and may reflect interspecific variation in ecology and behavior as well as intraspecific variation between captive and wild specimens. We compared trunk vertebrae bone microstructure in captive and wild xenarthran mammals to test the effects of ecology and captivity. We collected µCT scans of the last six presacral vertebrae in 13 fossorial, terrestrial, and suspensorial xenarthran species (body mass: 120 g to 35 kg). For each vertebra, we measured centrum length; bone volume fraction (BV.TV); trabecular number and mean thickness (Tb.Th); global compactness (GC); cross-sectional area; mean intercept length; star length distribution; and connectivity and connectivity density. Wild specimens have more robust trabeculae, but this varies with species, ecology, and pathology. Wild specimens of fossorial taxa (Dasypus) have more robust trabeculae than captives, but there is no clear difference in bone microstructure between wild and captive specimens of suspensorial taxa (Bradypus, Choloepus), suggesting that locomotor ecology influences the degree to which captivity affects bone microstructure. Captive Tamandua and Myrmecophaga have higher BV.TV, Tb.Th, and GC than their wild counterparts due to captivity-caused bone pathologies. Our results add to the understanding of variation in mammalian bone microstructure, suggest caution when including captive specimens in bone microstructure research, and indicate the need to better replicate the habitats, diets, and behavior of animals in captivity.

### KEYWORDS

axial skeleton, morphology, trabecular bone, vertebra, Xenarthra

**ABBREVIATIONS:** BV.TV, bone volume fraction; CL, centrum length; CSA, cross-sectional area; FMNH, Field Museum of Natural History; GC, global compactness; MANCOVA, multivariate analysis of covariance; MANOVA, multivariate analysis of variance; MIL, mean intercept length; PC, principal component; PCA, principal component analysis; ps, pre-sacral position; SLD, star length distribution; Tb.N, trabecular number; Tb.Th, trabecular thickness; TBA, trabecular bone architecture; VOI, volume of interest;  $\mu$ CT, micro-computed tomography.

#### 1 | INTRODUCTION

Many natural history collections include specimens acquired from zoos (captive specimens) in addition to those collected in their natural habitats (wild specimens). The presence of captive specimens in natural history collections allows researchers to access rare or endangered

taxa as well as those protected by the Convention on International Trade in Endangered Species, increasing the taxonomic breadth, size, and ontogenetic diversity of collections (Panagiotopoulou et al., 2016, 2019). Captive specimens must sometimes be used in research either due to a lack of wild specimen availability or to expand either the sample size or taxonomic breadth of a dataset (Panagiotopoulou et al., 2019). Additionally, captive specimens can be used as a point of comparison to wild specimens, allowing us to understand how lifetimes spent in zoo environments impact morphology and bone biology (King et al., 2011; Zuccarelli, 2004).

When used without taking captivity into account, data from captive specimens can be problematic in functional morphology research because of the highly contrasting lifestyles of captive and wild specimens. Zoo enclosures differ greatly from wild habitats: the enclosures provided are typically much smaller than wild ranges (O'Regan & Kitchener, 2005); the diets of zoo animals are often completely different from wild diets and sometimes include different macronutrient make-up (Crawshaw & Oyarzun, 1996); captive animals often grow faster and live longer than their wild counterparts because of diet and veterinary care (Shaw et al., 1987); captive animals often display stereotypies: repetitive behaviors with no goal or function (Mason, 1991); and there are pathologies seemingly unique to captive specimens (Crawshaw & Oyarzun, 1996; Panagiotopoulou et al., 2016, 2019). Additionally, many captive specimens lack complete or detailed histories. Although some zoo animals are born in the wild and placed in captivity later in life, even after living in captivity for a few months, their bone microstructure should reflect their captive habitat and behaviors (Barak et al., 2011).

Many studies have found differences in the bones of captive and wild specimens including ontogenetic patterning, gross morphology, and pathology (Armitage, 1983; Canington et al., 2018; Harbers et al., 2020; King et al., 2011; Zuccarelli, 2004), but these studies usually focus on gross morphology, cortical bone structure, or traditional histology. There have been no studies investigating the effects of captivity on bone microstructure, or more specifically, trabecular bone architecture (TBA), of mammals. Trabecular bone is the spongy bone tissue found in long bones, vertebrae, ribs, and elsewhere in the skeleton. In life, the cavities between the rod-like and plate-like trabeculae are filled with bone marrow and fat, and trabecular bone remodels in reaction to in vivo forces. Both the orientation and the magnitude of the forces acting on a bone affect its TBA (Barak et al., 2011; Huiskes et al., 2000; Kivell, 2016; Ruff et al., 2006; Willie et al., 2020). According to the theory of bone functional adaptation, TBA follows the principal stress trajectories generated from external loads experienced throughout an animal's

lifetime (Barak et al., 2011; Cowin, 1986; Huiskes et al., 2000; Kivell, 2016; Ruff et al., 2006; Sugiyama et al., 2010; Willie et al., 2020; Wolff, 1893). If the forces acting on an animal change, then the trabecular bone will adjust to the new force trajectories (Barak et al., 2011; Sugiyama et al., 2010). Because of this constant remodeling, TBA, and bone microstructure more generally, have the potential to provide important functional insights for rare or hard to access taxa or those with unusual gross morphologies (Smith & Angielczyk, 2020). However, because of the differences between zoo and wild environments, captive animals may experience different in vivo forces than their wild counterparts. These differences could affect the bone microstructure of captive specimens in ways that could mislead functional studies, but the potential severity of this problem is uncertain and needs to be examined.

To compare the bone microstructure of zoo and wild specimens, we chose a group of mammals with a large range of morphological and ecological diversity: the mammalian clade Xenarthra, which includes sloths, armadillos, anteaters, and their extinct relatives. Xenarthra consists of some of the most derived placental mammals, including taxa with specializations for completely suspensory lifestyles, myrmecophagous diets, and multiple types of forelimb digging (Clerici et al., 2018; Gaudin et al., 2018; Hayssen, 2009, 2010, 2011; Hayssen et al., 2012; Navarrette & Ortega, 2010; Rood, 1970).

One of the most functionally interesting regions of xenarthran mammals are their vertebrae. In addition to having an extra process on the posterior thoracic and lumbar vertebrae, the lumbar regions of their spines are functionally important (Figure 1) (Gaudin, 1999; Gaudin & Biewener, 1992; Gaudin & Nyakatura, 2018; Oliver et al., 2016). Xenarthrous vertebrae, when coupled with increased epaxial musculature, increase the range of motion and stiffness of the postdiaphragmatic region (Gaudin & Biewener, 1992; Gaudin & Nyakatura, 2018; Oliver et al., 2016). The lumbar region is loaded differently in each ecological group within Xenarthra, but all xenarthrans are united by their postdiaphragmatic musculoskeletal synapomorphies (Amson & Nyakatura, 2018; Gaudin, 1999; Gaudin & Nyakatura, 2018). Beyond the unique morphology of xenarthrous vertebrae, sloths and anteaters are known to experience soft tissue mineralization in captivity (Arenales et al., 2020; Crawshaw & Oyarzun, 1996; Han & Garner, 2016). All captive Tamandua specimens in the Field Museum of Natural History (FMNH) zoology collections have vertebral hyperostosis, a severe overgrowth of bone around the vertebrae and ribs (Crawshaw & Oyarzun, 1996). This pathology is caused by captive conditions but is not an inevitability of captivity. The impact of this and other bone pathologies of Xenarthrans on bone microstructure has not yet been examined.

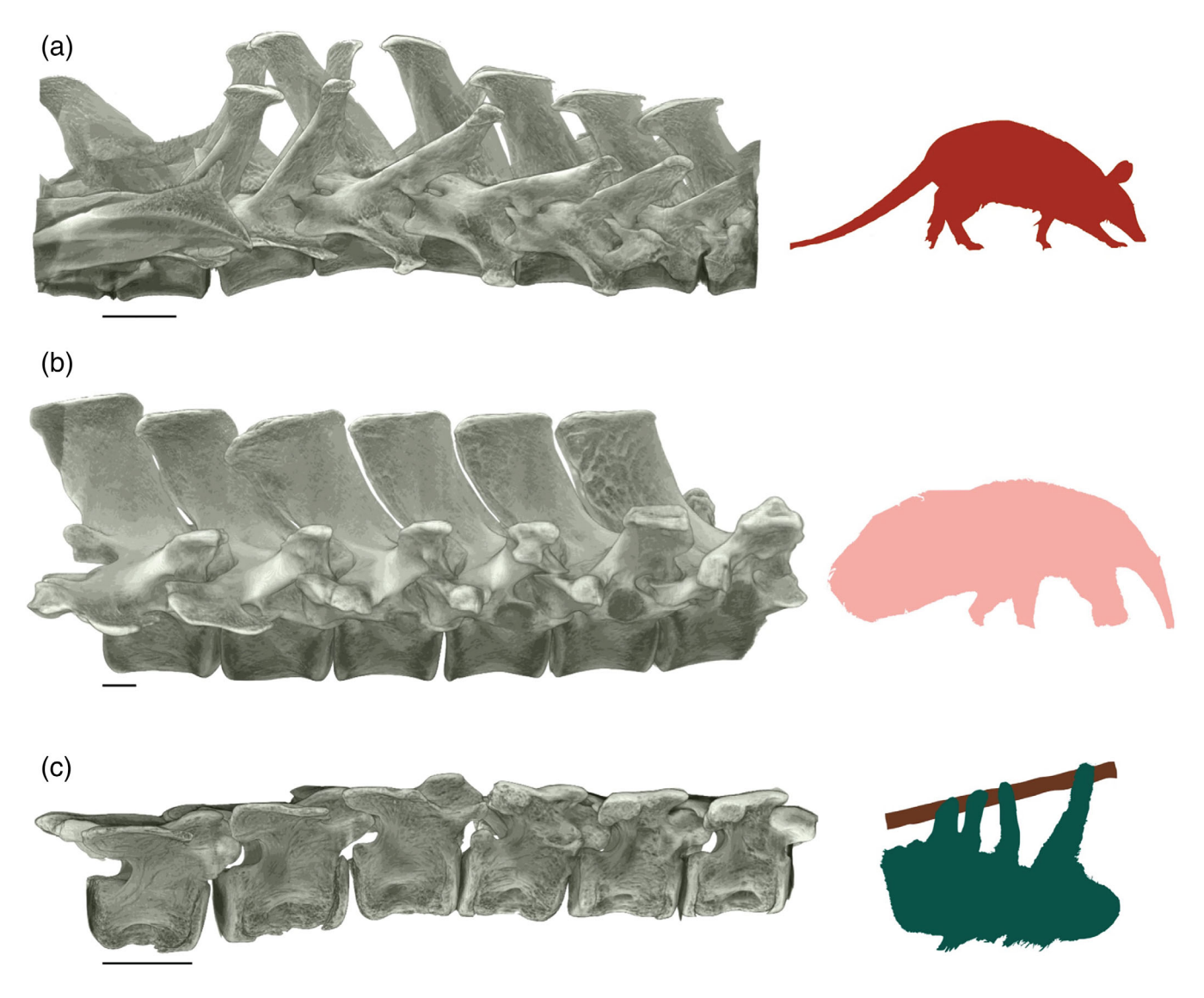


FIGURE 1 (a) 3D rendering of the tenth thoracic vertebra through the fifth lumbar vertebra of FMNH 60493 with silhouette of *Dasypus novemcinctus* (cranial to right). (b) 3D rendering of the twelfth thoracic vertebra to the second lumbar vertebra of FMNH 26563 with silhouette of *Myrmecophaga tridactyla* (cranial to right). (c) 3D rendering of the fourteenth thoracic vertebra to the third lumbar vertebra of FMNH 69589 with silhouette of *Bradypus variegatus* (cranial to right). Silhouettes are not to scale. Scale bars = 1 cm

To understand how the distinct in vivo loadings of the xenarthran lumbar vertebrae affect their morphology, we compared the bone microstructure of posterior thoracic and lumbar vertebrae of captive and wild specimens of 13 xenarthran species. In addition to spanning the entire size range of Xenarthra, our dataset includes much of its morphological and functional disparity, as well as the entire range of locomotor ecology in extant members of this clade. Our dataset can provide insight into the effects of captivity on the TBA of mammals with differing ecologies and that are subject to different physical constraints. This will allow us to understand the potential biases introduced by using captive specimens in functional studies of bone microstructure and make recommendations for best practices in future research.

### 2 | MATERIALS AND METHODS

### 2.1 | Specimen choice

We chose 44 xenarthran specimens, including 21 captive and 23 wild, from the FMNH mammalogy collections to undergo X-ray microcomputed tomography ( $\mu$ CT) scanning at the University of Chicago's PaleoCT facility (https://luo-lab.uchicago.edu/paleoCT.html). These specimens represent 13 species across 10 genera, span all three major xenarthran clades, and encompass much of the group's ecomorphological diversity and disparity (Table 1). Because TBA is affected by in vivo forces as well as development, we used only adult specimens (determined by fusion of the cranial sutures and long bone epiphyses) with full vertebral

columns (Gaudin & Biewener, 1992). Within the specimens we used, the number of lumbar vertebrae varied from two to five (Table 1). In order to include all lumbar vertebrae across all specimens and standardize across specimens, we scanned the last six presacral vertebrae (Figure 1). As a proxy for body size, we measured centrum length (CL) for each vertebra of interest; when close articulation of the vertebrae prevented use of the physical specimens, we measured 3D meshes of the vertebrae in Autodesk MeshMixer or ORS Dragonfly 2020.1 (Object Research Systems 2019).

### 2.2 | Scanning and analysis

We scanned all specimens using the 240 kV tube of the PaleoCT lab's GE v|tome|x  $\mu$ CT scanner at resolutions from 22.101 to 96.551  $\mu$ m (average resolution 44.899  $\mu$ m), depending on specimen size (Table 1). We reconstructed the scans in GE phoenix datos|x and aligned and cropped the reconstructed scans using VGstudio (Volume Graphics 2019). Following the method in Smith and Angielczyk (2020), we segmented prism-shaped volumes of interest (VOI) (Figure 2a). We determined the size and location of the prism by orienting the vertebra in cranial view and selecting the largest 2D square area of trabecular bone at the dorsoventrally and mediolaterally narrowest point of the centrum. This VOI included all possible trabecular bone craniocaudally without including any cortical bone. This

method ensures analysis of the largest possible volume of trabeculae with a consistent shape, no matter the shape or size of the vertebra (Figure 2a).

Using the "Threshold" tool in FIJI, we converted the VOI into a binary image stack in which we maximized bone sampling and minimized sampling of nonbone materials (Amson et al., 2017; Schindelin et al., 2012). We analyzed the binary image stack in Quant3D using a user-defined threshold of 127 to 255 as required by the software to define the binary colors; 2,049 uniform rotations; dense vectors and random rotations turned on; omit side intersecting paths turned on; and star volume and star length distributions (SLDs) calculated with 2,000 points (Ketcham, 2005; Ketcham & Ryan, 2004). We used the largest centered sphere that would fit within the rectangular VOI as the volume of interest for these calculations to eliminate edge-related artifacts (Figure 2a). Quant3D outputs several values for analysis including bone volume fraction (BV.TV), trabecular number (Tb. N), mean trabecular thickness (Tb.Th), and two measures of trabecular anisotropy (directionality): mean intercept length (MIL) and SLD (Figure 3). Additionally, we calculated connectivity and connectivity density (Conn.D) from these VOIs using the connectivity function in BoneJ macro in FIJI (Doube et al., 2010; Schindelin et al., 2012). We excluded any specimens with a connectivity of less than 40, a threshold chosen because of the small maximum possible VOI size obtainable in the smallest organisms in our dataset (Mielke et al., 2018). Together, the

**TABLE 1** Details of specimens sampled. Columns include ranges of the number of vertebrae. Thoracic vertebrae includes the mean in parentheses.

Taxon	Zoo specimens	Wild specimens	Thoracic vertebrae	Lumbar vertebrae	Scan resolutions (μm)
Bradypus tridactylus	0	1	15 (15)	3	46.833
Bradypus variegatus	1	3	16–17 (16)	3	41.997-45.906
Chlamyphorus truncatus	0	4	11–12 (12)	3	22.101–24.243
Choloepus hoffmanni	3	0	22-23 (22)	3–4	47.852–50.485
Choloepus didactylus	0	2	23 (23)	3–4	49.580-56.169
Cyclopes didactylus	3	3	15–16 (15)	2	25.031-26.123
Dasypus novemcinctus	2	3	10 (10)	5	38.878-42.931
Myrmecophaga tridactyla	2	2	15–16 (16)	2	93.178–96.551
Priodontes maximus	0	2	12-13 (13)	2	73.771–76.226
Tamandua mexicana	0	3	16–17 (17)	2–3	44.643-46.692
Tamandua tetradactyla	4	0	15-18 (17)	2–3	48.804-56.682
Tolypeutes matacus	2	1	12 (12)	3	27.465-30.597
Zaedyus pichiy	2	0	10-11 (11)	3–4	27.888-28.677

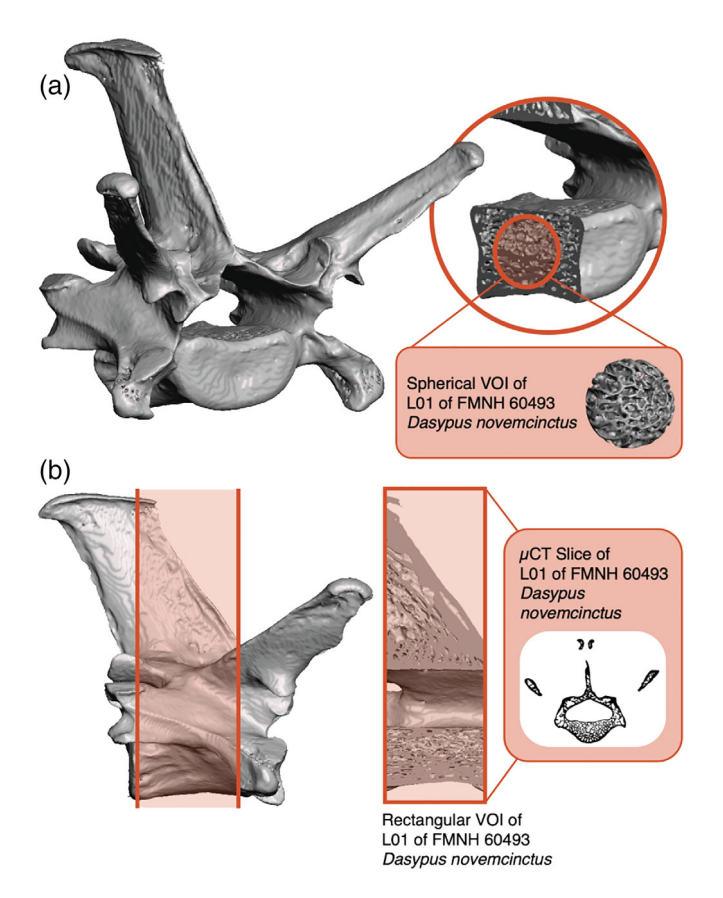


FIGURE 2 (a) 3D rendering of L01 of FMNH 60493 (*Dasypus novemcinctus*) with inset depicting the volume of interest used in TBA analyses as described in the text. (b) 3D rendering of L01 of FMNH 60493 (*Dasypus novemcinctus*) with the volume of interest used in the analysis of GC and CSA shaded in red. The inset depicts the VOI and a characteristic, binarized  $\mu$ CT slice

metrics we collected quantify important characteristics of the trabecular bone related to strength and trabecular direction (Silva & Gibson, 1997; Ulrich et al., 1999). In order to confirm the accuracy of our measurements, we calculated relative resolution (scan resolution/Tb.Th) and only included specimens with a relative resolution of greater than 2.5 (Kivell et al., 2011; Sode et al., 2008).

To analyze bone microstructure beyond TBA, we measured global compactness (GC) and cross-sectional area (CSA) for each vertebra using Amson's (2019) method (Figures 2b and 3). We segmented out entire vertebrae and binarized them using the same threshold as the VOI. Using the FIJI macro written by Amson (2019), we calculated CSA and GC for each vertebra including only the slices where the vertebral foramen was completely surrounded by bone (Figure (Amson, 2019; Doube et al., 2010; Schindelin et al., 2012). CSA measures the area of bone in each slice including both cortical bone and trabecular bone. GC measures the CSA of the bone divided by the total CSA (Amson, 2019).

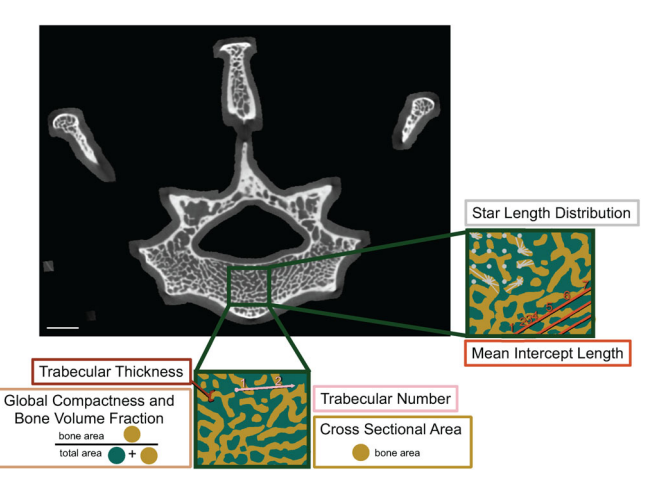


FIGURE 3 Representative  $\mu$ CT slice of T10 of FMNH 60493 (*Dasypus novemcinctus*). Dark green boxes indicate the region of interest. The inset regions of interest include trabecular bone (yellow) and intertrabecular space (teal). Star length distribution is calculated by measuring the length of trajectories from where points on a randomly translated point grid are within the trabeculae, as shown in light gray (Vesterby et al., 1989). Mean intercept length is the number of places where the lines of a randomly translated linear grid intersect with the interface between trabecular bone and intertrabecular space (in bright red) (Odgaard, 1997). Trabecular number is calculated by the method approximated using the pink arrow. Trabecular thickness is indicated by the dark red lines. The calculations used for bone volume fraction, global compactness, and cross-sectional area are shown in the tan and teal boxes. Scale bar = 2 mm. T, thoracic

We visualized major patterns of variation in our dataset of BV.TV, Tb.N, Tb.Th, GC, CSA, CL, MIL, SLD, connectivity, and Conn.D with principal component analysis (PCA) in R using R-Studio, tidyverse, ggbiplot, and ggplot2 packages (Vu et al., 2011; Wickham, 2016; Wickham et al., 2019; RStudio Team, 2020; R Core Team, 2020). Different permutations of the PCA included the entire data set, only the zoo specimens, and only the wild specimens, and we grouped specimens by locomotor ecology, genus, and captivity status.

To directly compare all eight numerical variables between captive and wild specimens, we created plots for BV.TV, Tb.N, Tb.Th, GC, CSA, MIL, SLD, connectivity, Conn.D, CL, and VOI size along the vertebral column for each genus (Figures 4 and S4–S13). This allowed us to visualize potential patterns along the vertebral column without obscuring possible effects of sample size. For a more direct comparison, we made boxplots for each of the numeric variables with separate panels for zoo and wild specimens of each genus (Figures S2 and S3). We made all of these visualizations using ggplot2 in RStudio (Wickham, 2016; RStudio Team, 2020).

## Bone Volume Fraction (Captive or Wild)

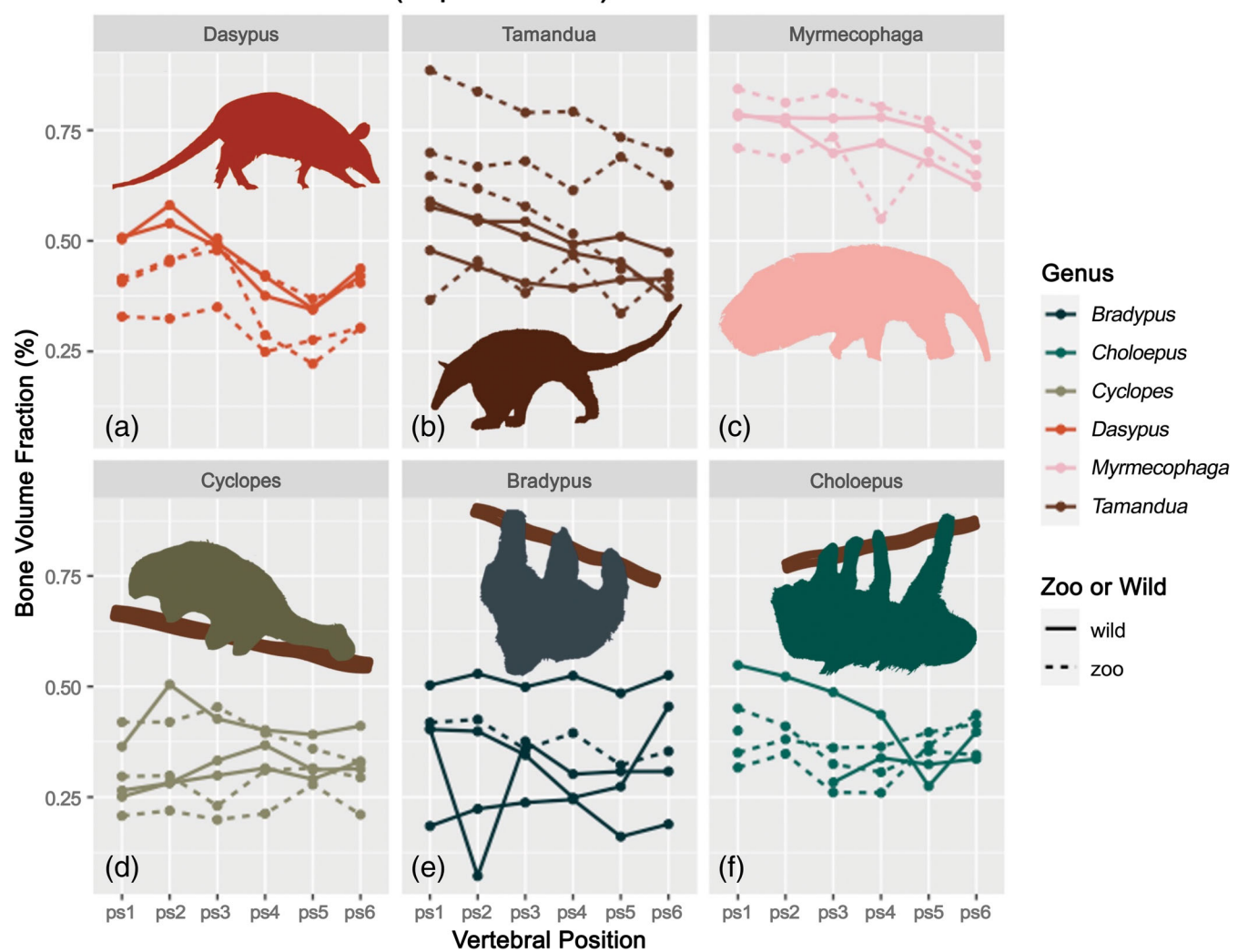


FIGURE 4 Bone volume fraction of six genera with silhouettes of each animal. Vertebral position starts in the thoracic column and ends at the last lumbar vertebra (ps6; see text for details). Dots indicate the BV.TV value at each vertebral position. Each line represents a single specimen. Silhouettes are not to scale

To statistically compare the captive and wild specimens, we used phylogenetic multivariate analysis of covariance (MANCOVA) with BV.TV, Tb.N, Tb.Th, GC, CSA, MIL, SLD, Connectivity, and Conn.D as the numeric variables, CL as the covariate (to assess influence of body size), and ecology and captivity status as categorical variables. Because our dataset includes measurements from multiple vertebral positions, we repeated this analysis for each vertebral position. We pruned the time-scaled tree from Gibb et al. (2016) to include only the species in our dataset (Gibb et al., 2016). We added captive operational taxonomic units to this tree as branches of negligible length that are sister groups to the species that included both captive and wild specimens (Figure S1). The addition of negligible length branches could result in a poorer fit of the evolutionary

model used to estimate phylogenetic covariance, which is potentially a limitation (Revell, 2010). However, we consider this a reasonable trade-off that enables us to consider phylogeny in our analyses. We prepared the data for the MANCOVA by calculating the species means of each metric by vertebral position. Before conducting the analyses, we scaled all of the data using the scale() function in base R (R Core Team, 2020). We conducted phylogenetic MANCOVAs using a Wilks Lambda test and Brownian motion within the mvgls() and manova.gls() functions in the mvMORPH package in R using RStudio (Clavel et al., 2015; R Core Team, 2020; RStudio Team, 2020). The models used for each MANCOVA are listed in Table 2.

In our dataset, ecological partitions are very similar to phylogenetic divisions, potentially skewing the phylogenetic MANCOVA results. To better understand the effects of

 TABLE 2
 Phylogenetic multivariate analysis of covariance (MANCOVA) results

Position for analysis	Model examined	Factor	Test statistic	Wilks lambda $p$ -value ( $\alpha \leq 0.05$
1	CL + captivity	CL	0.01072	0.000999*
		Captivity	0.01788	0.000999*
	CL + ecology	CL	0.03695	0.005994*
		Ecology	0.86794	0.537463
	${\rm CL}+{\rm captivity}*{\rm ecology}$	CL	0.009068	0.000999*
		Captivity	0.015305	0.000999*
		Ecology	0.577159	0.273726
		Captivity*ecology	0.109946	0.047952*
2	CL + captivity	CL	0.004920	0.000999*
		Captivity	0.01123	0.000999*
	CL + ecology	CL	0.02246	0.000999*
		Ecology	0.76217	0.347652
	${\rm CL}+{\rm captivity*ecology}$	CL	0.008859	0.000999*
		Captivity	0.016304	0.000999*
		Ecology	0.495741	0.223776
		Captivity*ecology	0.147411	0.047952*
3	CL + captivity	CL	0.003540	0.000999*
		Captivity	0.008978	0.000999*
	CL + ecology	CL	0.037110	0.000999*
		Ecology	0.88517	0.649351
	CL + captivity*ecology	CL	0.006082	0.000999*
		Captivity	0.004283	0.000999*
		Ecology	0.484653	0.248751
		Captivity*ecology	0.114548	0.034965*
Į.	CL + captivity	CL	0.003790	0.000999*
		Captivity	0.004283	0.000999*
	CL + ecology	CL	0.03838	0.000999*
		Ecology	0.85816	0.516484
	CL + captivity*ecology	CL	0.005604	0.000999*
		Captivity	0.008675	0.000999*
		Ecology	0.397705	0.187812
		Captivity*ecology	0.183412	0.056943
5	CL + captivity	CL	0.003439	0.000999*
		Captivity	0.005696	0.000999*
	CL + ecology	CL	0.02564	0.000999*
		Ecology	0.83140	0.444555
	CL + captivity*ecology	CL	0.01233	0.000999*
		Captivity	0.02128	0.000999*
		Ecology	0.60582	0.303696
		Captivity*ecology	0.15972	0.061938
5	CL + captivity	CL	0.006289	0.000999*
	•	Captivity	0.005240	0.000999*
	CL + ecology	CL	0.02815	0.000999*

TABLE 2 (Continued)

Position for analysis	Model examined	Factor	Test statistic	Wilks lambda <i>p</i> -value ( $\alpha \leq 0.05$ )
		Ecology	0.78065	0.34656
	CL + captivity*ecology	CL	0.01380	0.000999*
		Captivity	0.02718	0.000999*
		Ecology	0.68073	0.336663
		Captivity*ecology	0.44150	0.169830

<sup>\*</sup>indicates significance ( $\alpha \le 0.05$ ).

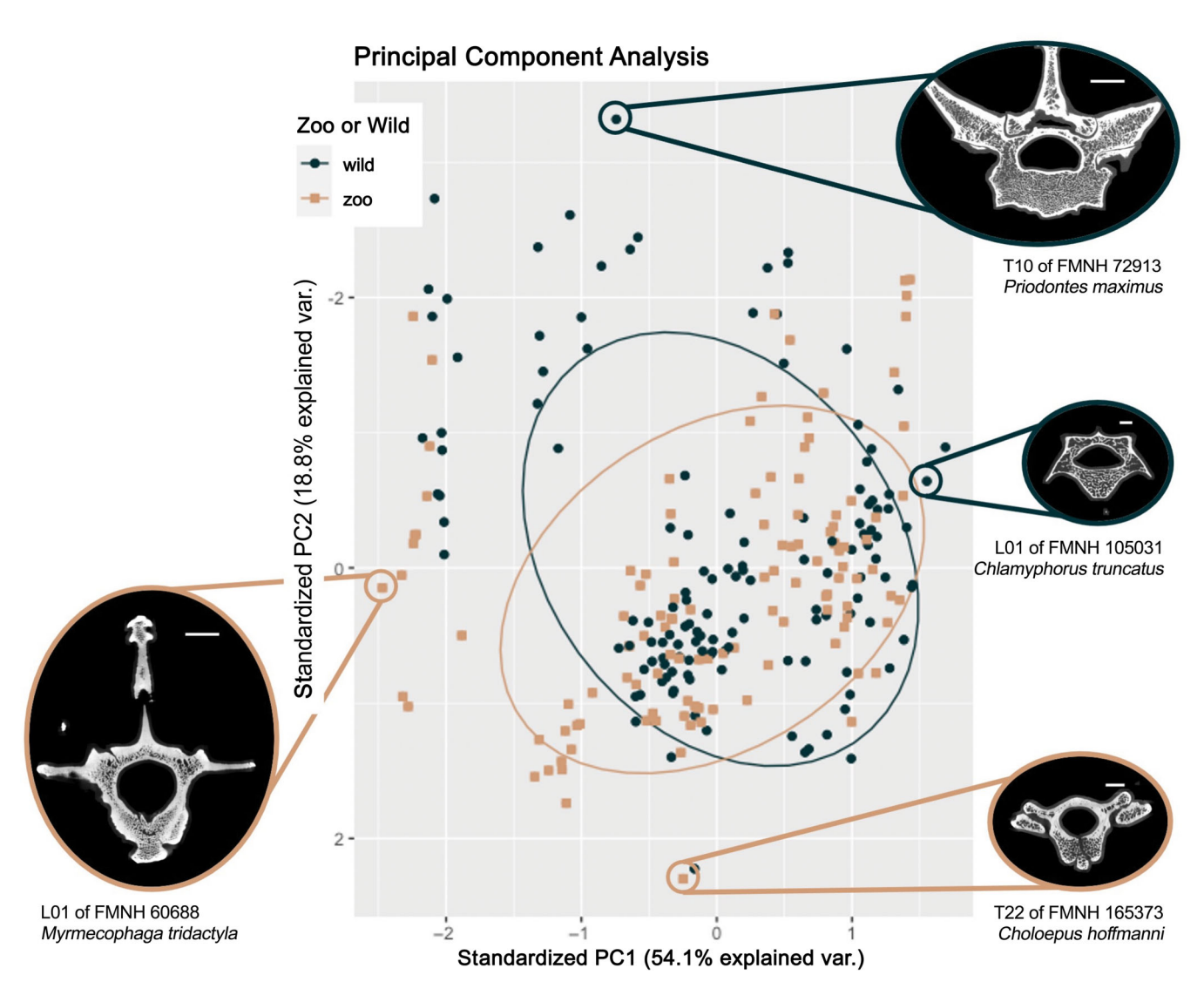


FIGURE 5 Principal component analysis of all specimens with representative vertebrae at the extremes of each axis. Captive specimens are represented by pink squares and wild specimens by navy dots. Scale bars for *Myrmecophaga tridactyla* and *Priodontes maximus* are 1 cm. Scale bar for *Choloepus hoffmanni* is 5 mm. L, lumbar; T, thoracic

captivity and patterning along the vertebral column within ecological groups, we used the npmv package in R to perform nonparametric multivariate analysis of variances (MANOVAs) for four genera with relatively large sample sizes: *Dasypus*, *Cyclopes*, *Choloepus*, and *Tamandua* 

(Bathke et al., 2008; Ellis et al., 2017; R Core Team, 2020; RStudio Team, 2020). We used captivity status and position for analysis as the categorical variables with BV.TV, Tb.N, Tb.Th, GC, CSA, CL, MIL, SLD, Connectivity, and Conn.D as the numeric variables.

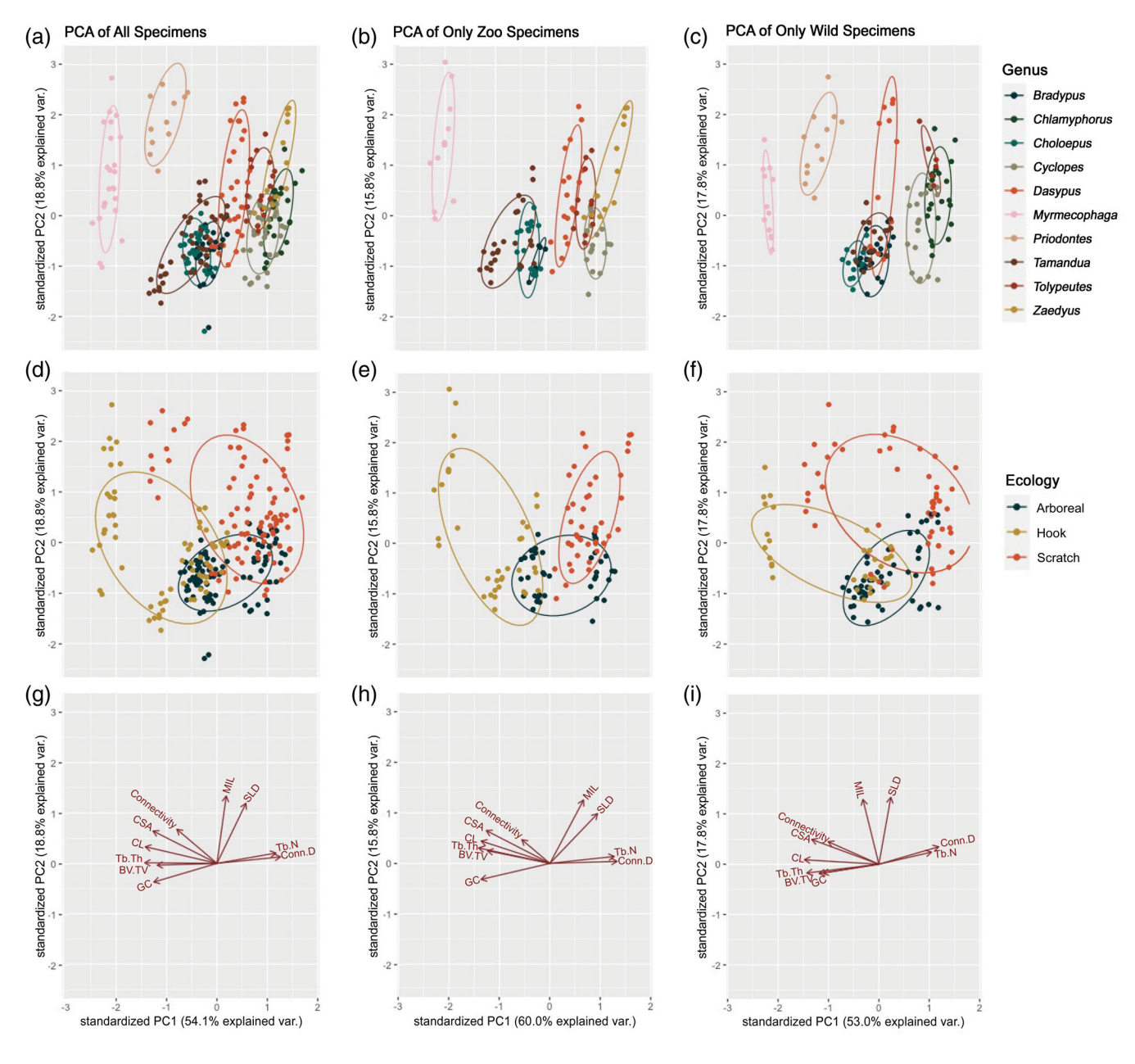


FIGURE 6 Principal component analyses: (a) All specimens, grouped by genus. (b) Zoo specimens, grouped by genus. (c) Wild specimens, grouped by genus. (d) All specimens, grouped by ecology. (e) Zoo specimens, grouped by ecology. (f) Wild specimens, grouped by ecology. (g) Biplot of all specimens. (h) Biplot of zoo specimens. (i) Biplot of wild specimens

### 3 | RESULTS

### 3.1 | Principal component analysis

### 3.1.1 | All-specimen PCA

The first principal component (PC1) of all specimens explains 54.1% of the variance and is primarily defined by BV.TV, CL, Conn.D, Tb.N, and Tb.Th (Figures 5, 6a,d,g, and S15; Table S1). PC2 explains 18.8% of the variance and is primarily defined by MIL and SLD. PC3 through

PC10 cumulatively account for only 27.06% of the variance and do not reveal any noteworthy patterns when plotted against each other. Examples of specimens falling near the extremes of each PC axis are shown in Figure 5. Vertebrae that fall in the upper left quadrant are characterized by high CL, high BV.TV, high CSA, and high connectivity. The vertebrae in the upper right quadrant are characterized by high MIL and SLD, high Tb.N, high Conn.D, and lower CL. The lower right quadrant holds the most vertebrae. Those vertebrae are characterized by lower CL, low MIL and SLD, low GC, and high Tb.N.

There are very few vertebrae that fall in the lower left quadrant, but they are characterized by high BV.TV, lower MIL and SLD, and higher GC.

The PCA performed on all specimens reveals few patterns when specimens are grouped by zoo and wild categories (Figure 5). The two groups occupy similar locations within the PC space but have different primary axes of variation that are perpendicular to each other: the zoo specimens vary more along PC1 whereas the wild specimens vary more along PC2.

Further patterns emerge when specimens are grouped by genus and ecology (Figure 6a,d). Each genus occupies a defined region of the PC space, but some genera overlap (Figure 6a). Overall, intrageneric variation occurs along PC2 whereas intergeneric variation occurs along PC1. Myrmecophaga and Priodontes both occur in the upper left quadrant of the PC space with *Priodontes* occupying higher values of both PC1 and PC2. Dasypus occupies more than half of PC2, but a much smaller range of PC1. Zaedyus, Tolypeutes, Cyclopes, and Chlamyphorus fall within the positive half of PC1 and have much larger ranges along PC2, somewhat echoing the pattern seen in Dasypus. Choloepus and Bradypus occupy the smallest ranges, falling just below the origin of the PC space. Tamandua has a larger range across PC1 than any other genus. Grouping the all-specimen PC space by ecology results in three overlapping regions (Figure 6d). The arboreal specimens occupy the smallest range, near the origin. The hook-and-pull digging specimens occupy the largest range, covering more than half of PC1 and PC2. The scratch digging specimens display about the same amount of variation as the hook-and-pull diggers along PC2, but have much less variation along PC1, most of which falls on the positive half of the PC space.

### 3.1.2 | Captive specimen PCA

In the captive specimen PC space, PC1 explains 60.0% of the variance and is primarily defined by Tb.N, Tb.Th, and Conn.D. It is secondarily defined by CSA, BV.TV, CL, and GC (Figure S15). PC2 explains 15.8% of the variance and is primarily defined by MIL and SLD (Figure 6h and S15). However, MIL and SLD have higher loadings for PC1 in the captive analysis than in the all-specimen analysis. PC3 through PC10 cumulatively account for only 24.19% of the variance and do not reveal any noteworthy patterns when plotted against each other. The vertebrae in the upper left quadrant are characterized by high CSA, high BV.TV, high CL, high Tb.Th, and high connectivity. The upper right quadrant is characterized by high MIL and SLD, high Tb.N, high Conn.D, and low CL. The lower right quadrant contains the majority of vertebrae

and is characterized by low CL, high Tb.N, high Conn.D, and low MIL and SLD. The lower left quadrant has the fewest vertebrae. These specimens are characterized by high GC, high BV.TV, low Tb.N, and low MIL and SLD.

As in the all-specimen PC space, intrageneric variation lies along PC1 whereas intergeneric variation lies along PC1. The range of *Tamandua* differs the most from the all-specimen PC space (Figure 6b). In the captive specimen PC space, *Tamandua* occupies a smaller range of PC1 values while maintaining a similar range along PC2. *Myrmecophaga* vertebrae are the only vertebrae found in the upper left quadrant of the PC space. They have much more variation along PC2 than PC1. *Dasypus*, *Tolypeutes*, *Zaedyus*, and *Cyclopes* occupy similarly shaped regions of morphospace as seen in the all-specimen PC space although the absolute sizes of these spaces are smaller. *Bradypus* and *Choloepus* group in the lower right quadrant, close to the origin.

Grouping zoo specimens by ecology results in more distinct groups with smaller ranges than in the all-specimen space (Figure 6e). The scratch digging specimens have a much smaller range than in the all-specimen space. Their variation is primarily along PC2 whereas they remain entirely on the positive half of PC1. Arboreal specimens again group in the lower right quadrant, near the origin, but with a slightly larger range than in the all-specimen PC space. The hook-and-pull digging specimens have the largest range with variation along almost all of PC2 but only along the negative values of PC1.

### 3.1.3 | Wild specimen PCA

PC1 of the wild specimen PC space explains 53.0% of the variance (Figure 6c,f,i; Table S1). It is primarily defined by Tb.N, Conn.D, and CL and secondarily defined by Tb. Th, BV.TV, GC, and CSA. PC2 explains 17.8% of the variance and is defined by MIL and SLD. PC3 through PC10 cumulatively account for only 29.22% of the variance and do not reveal any noteworthy patterns when plotted against each other. When grouped by genus, PC2 explains most of the intraspecific variation whereas PC1 explains most of the interspecific variation (Figure 6c). The vertebrae in the upper left quadrant of the wild specimen PC space are characterized by high CSA, high CL, high connectivity, and high MIL and SLD. The upper right quadrant contains vertebrae with high Tb.N, high MIL and SLD, high Conn.D, and low CL. Most of the vertebrae are found in the lower right quadrant and have high Tb.N, low CL, and low MIL and SLD. The fewest vertebrae are found in the lower left quadrant. They have high GC, high BV.TV, high CL, and high Tb.Th.

Myrmecophaga occupies a much smaller range than in the other PC spaces, with variation along the middle of PC2 and the negative values of PC1. Priodontes occupies a slightly larger range in the wild PC space than in the all-specimen PC space, but it is centered in the same place on the plane. Chlamyphorus, Tolypeutes, and Cyclopes still occupy very narrow ranges along PC1 and larger ranges of PC2. Dasypus occupies the largest range along PC2, spanning almost the entire range of data points while having a relatively small range along PC1. Bradypus, Choloepus, and Tamandua have overlapping ranges close to the origin, but within the lower right quadrant.

Ecological groups overlap more in the wild specimen PCA than in the captive specimen PCA and the all-specimen PCA (Figure 4f). The arboreal specimens have the smallest area of the PC space, which is the same shape as that occupied by the arboreal specimens in the all-specimen PC space. The scratch diggers occupy the largest range, covering the positive values of PC1 and PC2. Hook-and-pull diggers occupy a small range of PC2 near the axis but a large range of PC1 within the negative half of the PC space.

### 3.2 | MANOVA and MANCOVA

When considering the entire dataset, body size and captivity status have a significant impact ( $\alpha \leq 0.05$ ), on bone microstructure for all models (Table 2). The bone microstructure of captive and wild specimens differ significantly for all vertebral positions with body size as a covariate when compared as a whole dataset (Table 2). Body size also has a significant impact on bone structure when captivity and body size are used as factors. The three ecological groups, arboreal, scratch digging, and hook-and-pull digging, are not significantly different for any vertebral position or model (Table 2). However, when body size, captivity status, and ecology are

considered, captivity\*ecology is only significant for the first three vertebral positions included in this analysis (Table 2).

When comparing captivity status within genera, Tamandua (p=0.013) and Dasypus (p=0.008) had significantly different captive and wild bone microstructure (Table 3). The bone microstructure of captive Choloepus (p=0.284) and Cyclopes (p=0.118) specimens did not differ significantly from the wild specimens (Table 3). Vertebral position significantly impacted the bone microstructure of Dasypus specimens (p=0.015). Vertebral position was not significant for any other genus examined (Table 3).

### 3.3 | Direct comparisons

BV.TV was the most informative metric for direct comparisons between zoo specimens and wild specimens and for visualizing patterns along the vertebral column (Figure 4; see Figures S4-S14 for trajectories of all metrics and all genera). In the PCA of all specimens, BV.TV lies almost exactly along PC1 with higher BV.TV in the negative direction. Because some of the genera are represented by only captive specimens, only wild specimens, or by very few specimens, our comparisons focus on Dasypus, Myrmecophaga, Tamandua, Cyclopes, Bradypus, and Choloepus (Figure 4). These genera show differing patterns of variation in BV.TV along the vertebral column, and the type and magnitude of the effect of captivity also varies by genus. BV.TV in Dasypus consistently increases to a peak at pre-sacral position ps2 or ps3, then decreases to a minimum at ps4 or ps5 before slightly increasing at the end of the vertebral column (Figure 4a). This pattern is followed in all of the specimens we measured, but the zoo specimens have lower BV.TV than wild specimens (Figure 4a). The two wild specimens follow almost exactly the same trajectory whereas the three zoo specimens have a larger range (22.1–50.5% for zoo specimens;

TABLE 3 Nonparametric multivariate analysis of variances (MANOVAs) by genus

Genus	Factors examined	Degrees of freedom	Wilks lambda permutation <i>p</i> -value ( $\alpha \le 0.05$ )
Dasypus	Captivity	1	0.008*
	Position for analysis	5	0.015*
Cyclopes	Captivity	1	0.118
	Position for analysis	5	0.981
Tamandua	Captivity	1	0.013*
	Position for analysis	5	0.619
Choloepus	Captivity	1	0.284
	Position for analysis	5	0.385

<sup>\*</sup>indicates significance ( $\alpha \le 0.05$ ).

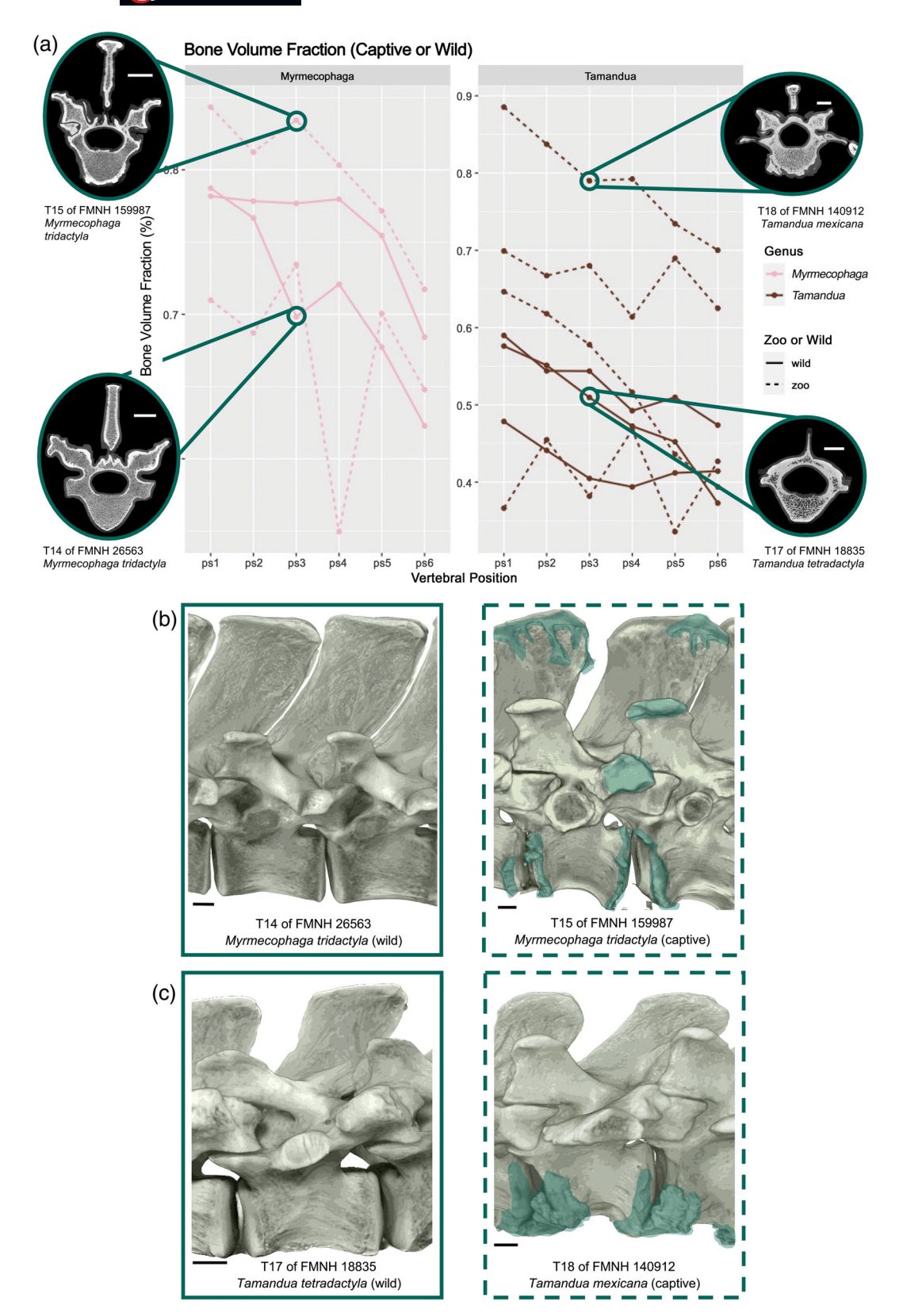


FIGURE 7 (a) Bone volume fraction of *Myrmecophaga* and *Tamandua* specimens. CT slices are example captive or wild vertebrae (dorsal to top). Each line represents a single specimen. Scale bars for *Myrmecophaga* are 1 cm. Scale bars for *Tamandua* are 5 mm. (b) 3D renderings of example captive and wild *Myrmecophaga* vertebrae with captive specimen surrounded by a dashed box (cranial to left). Pathology on the captive vertebrae is highlighted in teal. Scale bars = 5 mm. (c) 3D renderings of example captive and wild *Tamandua* vertebrae with captive specimen surrounded by a dashed box (cranial to left). Pathology on the captive vertebrae is highlighted in teal. Scale bars = 4 mm. L, lumbar; T, thoracic

34.4–58.1% for wild specimens) (Figures S2 and S3). In *Dasypus*, wild specimens have higher ranges for Tb.N, GC, MIL, and SLD (Figure S3).

In most *Myrmecophaga* specimens, BV.TV decreases consistently along the vertebral column (Figure 4b). One zoo specimen has higher BV.TV than the wild specimens and one zoo specimen has lower BV.TV than the wild specimens with a minimum BV.TV at ps4. BV.TV ranges from 55.0 to 84.3% for captive specimens and from 67.7 to 78.0% for wild specimens. Captive specimens of *Myrmecophaga* have a higher range of Tb.Th and GC than wild specimens (Figure S2). *Myrmecophaga* captive specimens have a lower range of Tb.N, CSA, and MIL than wild specimens (Figure S3). All of the captive specimens of *Myrmecophaga* that we examined had a bone pathology that likely affected their bone microstructure (Figure 7).

BV.TV decreases along the vertebral column in most *Tamandua* specimens (Figure 4c). Although this pattern holds for most specimens, two zoo specimens have much more chaotic trajectories, one peaking at ps4 and the other at ps5. Three of the zoo specimens have higher BV. TV than the wild specimens, but one zoo specimen mostly lies within the range of wild specimens. The wild specimens follow similar trajectories and have a small range of values, whereas the zoo specimens have a

very large range (33.6–88.5% for zoo specimens and 37.3–59.0% for wild specimens). Captive specimens of *Tamandua* have larger ranges for all of the numeric variables except SLD and Conn.D (Figure S3). Tb.Th, GC, and CSA are higher in captive specimens than in wild specimens whereas Tb.N is higher in wild specimens (Figures S3 and S5–S8). The differences in range and pattern are likely due to vertebral hyperostosis (Crawshaw & Oyarzun, 1996), a pathology seen in all of the *Tamandua* zoo specimens in our dataset and in the FMNH mammalogy collections as a whole (Figures 7 and 8).

Unlike in *Dasypus*, *Myrmecophaga*, and *Tamandua*, BV.TV in *Cyclopes*, *Bradypus*, and *Choloepus* has no clear patterning along the vertebral column and no clear difference between zoo and wild specimens. *Cyclopes* specimens all have different patterns along the vertebral column (Figure 4d). Zoo specimens of *Cyclopes* tend to have lower BV.TV than wild specimens (12.9 to 45.4% for zoo specimens and from 25.1 to 50.4% for wild specimens), but this pattern is less consistent than in *Dasypus*. The ranges for Tb.N, Tb.Th, CSA, MIL, and CL are very similar for captive and wild specimens of *Cyclopes* (Figures S2 and S3). *Bradypus* specimens have no clear pattern along the vertebral column (Figure 4e). The single zoo specimen of *Bradypus* falls within the range of

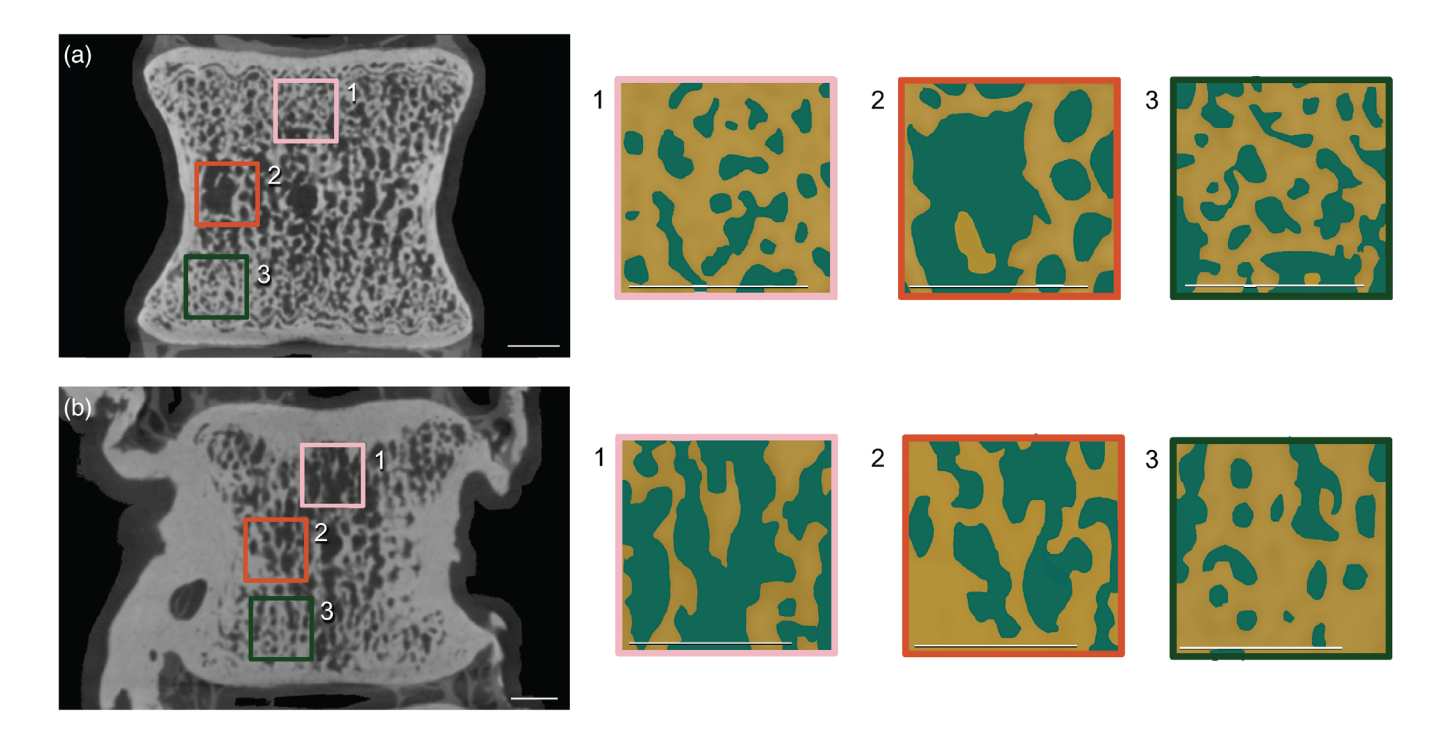


FIGURE 8 (a)  $\mu$ CT scan slice of L1 of wild *Tamandua mexicana* FMNH 18835 with three inset boxes demonstrating how the density of trabecular bone changes along the vertebral centrum (cranial to top). Inset boxes are recolored representations of trabecular bone with bone in yellow and intertrabecular space in teal. (b)  $\mu$ CT scan slice of L1 of captive *Tamandua tetradactyla* FMNH 186913 with three inset boxes demonstrating how the density of trabecular bone changes along the vertebral centrum (cranial to top). Inset boxes are recolored representations of trabecular bone with bone in yellow and intertrabecular space in teal. Scale bars = 2 mm. L, lumbar

the wild specimens. BV.TV ranges from 32.2 to 42.5% in zoo specimens and from 7.17 to 52.9% in wild specimens. The ranges of other numeric variables look different between captive and wild specimens but there is only one captive specimen of *Bradypus*, making the ranges of zoo specimens much smaller (Figure S3). The BV.TV of *Choloepus* specimens show unpredictability along the column similar to *Bradypus* (Figure 4f). BV.TV ranges from 21.6 to 45.1% in zoo specimens and from 27.5 to 54.9% in wild specimens. The ranges of captive and wild specimens for each metric overlap almost entirely (Figure S3). The ranges for wild specimens tend to be smaller than the captive specimen ranges, but this is likely due to the difference in sample size between the two groups.

### 4 | DISCUSSION

In this work, we compared the bone microstructure of the vertebrae between wild and captive xenarthran specimens. We found that captivity has a significant impact on the bone microstructure of these organisms, but that the differences between the bone microstructure of captive and wild specimens are taxonomically variable and depend on locomotor ecology, body size, and pathology (Table 2). Nonpathological zoo specimens tend to have lower BV.TV, Tb. N, and GC than their wild counterparts, but this varies with species, vertebral position, and ecology (Figures 4, S4, S6 and S7). These metrics imply that wild specimens have stronger trabecular bone (Huiskes et al., 2000; Kivell, 2016; Silva & Gibson, 1997). Bone microstructure in captive specimens also varies in less predictable patterns along the vertebral column, possibly due to lower activity levels and stereotypies (Joo et al., 2003; Mason, 1991; Ruff et al., 2006; Willie et al., 2020).

The digging genera, Dasypus, Tamandua, Myrmecophaga have the clearest difference between captive and wild specimens (Table 3). Dasypus novemcinctus, the nine-banded armadillo, is a mid-sized armadillo that uses scratch-digging as its primary foraging technique (Clerici et al., 2018; Olson et al., 2016). The consistent pattern of BV.TV along the vertebral column implies that there are similar force loadings between individuals (Figure 4a). The activities performed in life seem to have the same loading pattern regardless of captivity, but a lower magnitude of force could cause the lower values of BV.TV in captive specimens (Guo & Kim, 2002; Huiskes et al., 2000). Because of their restricted environment, captive Dasypus likely forage less, and less strenuously than their wild counterparts (Ancona & Loughry, 2009; Clerici et al., 2018). This is probably related to their lower mean BV.TV, Tb.Th, GC, and MIL when compared to wild specimens (Figures S3-S5, S7, and S9). The lower activity

level inherent in a captive lifestyle would decrease external loads on their vertebrae, likely resulting in less robust trabeculae (Joo et al., 2003; Ruff et al., 2006). This expectation is supported by the significant difference (p=.008) between captive and wild specimens in a nonparametric MANOVA (Table 3). More detailed behavioral comparison between wild and captive *Dasypus* will help establish the causality of this relationship.

One would expect a similar pattern of decreased BV. TV in zoo specimens of Tamandua, the lesser anteater. This anteater is both a digger and an arborealist with a prehensile tail. It uses hook-and-pull digging to forage for termites and other colonial insects in the ground, in trees, and in termite mounds (Hayssen, 2011; Navarrette & Ortega, 2010). Although the body size and activity level of Tamandua are comparable to those of Dasypus, the two genera exhibit distinct patterns in their vertebral gross morphology and microstructure: the pattern along the vertebral column has a more linearly decreasing trajectory in Tamandua, and the zoo specimens of Tamandua have a much larger range of BV.TV than Dasypus (Figure 4b). This is at least partially due to the fact that all captive specimens of Tamandua in the FMNH mammalogy collection present vertebral hyperostosis, an overgrowth of bone on the ribs and vertebrae (Figure 7). Vertebral hyperostosis is caused by hypervitaminosis A. When captive Tamandua are given food with too much vitamin A and vitamin D, they experience an overgrowth of bone on their ribs and trunk vertebrae, causing pain, kyphosis, and occasionally hind limb paralysis (Crawshaw & Oyarzun, 1996). Mineralization of soft tissue and vertebral hyperostosis has been reported in both captive and wild anteaters in Brazil and in captive sloths (Arenales et al., 2020; Han & Garner, 2016).

Vertebral hyperostosis presents as somewhat jagged sections of bone on the vertebral centra and on the ribs (Figure 7c). This bone is made up of entirely compact bone; the original outline of the centrum is clearly visible in the  $\mu$ CT slices (Figure 7a). In addition to the external indications of vertebral hyperostosis, this pathology causes changes in the bone microstructure that have not been reported in previous work. There is a significant difference (p = .013) between the bone microstructure of captive and wild Tamandua vertebrae (Table 3). Captive Tamandua have TBA with higher Tb.Th, BV.TV, and GC, and lower Tb.N, and a much larger range of MIL than their wild counterparts (Figures S3–S7 and S9). The trabeculae are thicker with no consistent anisotropic pattern (Figures 6a and S10). The captive specimens of Tamandua have a much larger range of BV.TV than any of the other genera (Figure 4a). In healthy Tamandua vertebrae, there is a craniocaudal gradient of BV.TV, with smaller intertrabecular spaces closer to the epiphyses

and larger intertrabecular spaces toward the middle of the vertebral centrum, further from the epiphyses (Figure 8a). *Tamandua* vertebrae with vertebral hyperostosis lack this gradient: the intertrabecular space varies throughout the vertebral centrum with no gradient or pattern along the craniocaudal axis (Figure 8b). The differences in the bone microstructure of these anteaters are possibly due to a combination of effects of the pathology and the secondary effects of the pathology on activity level and activity type (Crawshaw & Oyarzun, 1996).

Myrmecophaga tridactyla, the giant anteater, is a hook-and-pull digger that primarily eats ants. It is largebodied and highly active in the wild, using knuckle walking to roam across large home ranges (Gaudin et al., 2018). BV.TV for Myrmecophaga decreases along the vertebral column for all specimens, similar to the pattern seen in Dasypus (Figure 4c). Giant anteaters are common in zoos, but in captivity they are fed much richer diets, are kept in enclosures far smaller than their native ranges, grow more quickly, and occasionally develop bone pathologies on their trunk vertebrae (Figure 7b) (Shaw et al., 1987). The lack of space, lower activity level, diet, pathology, and stereotypies all likely contribute to the more unpredictable patterns of BV.TV for captive specimens, similar to those seen in Tamandua (Figure 7a). These similarities likely also lead to similar patterns in Tb.Th, Tb.N, and GC for these two genera of anteaters: the range of Tb.Th is far larger for zoo specimens than for wild specimens; zoo specimens of both genera have lower Tb.N than wild specimens; and GC consistently decreases along the vertebral column, with zoo specimens having higher GC than wild specimens (Figures S3, S5–S7). Their larger body size likely accounts for the fact that their BV.TV is far higher than the other specimens examined here (Amson & Bibi, 2021). Because there are no healthy, captive individuals of Tamandua or Myrmecophaga available to us, disentangling the impact of captivity from the impact of this bone pathology is not possible. Captivity could have impacts on bone microstructure beyond the effects of vertebral hyperostosis or osteoarthritis, but further studies including healthy captive individuals are needed to address this.

The other three genera used to compare captive and wild individuals have little discernible pattern either along the vertebral column or between captive and wild specimens. The clearest pattern of the three belongs to *Cyclopes didactylus*, the silky anteater. This very small anteater is arboreal with a prehensile tail, eating ants foraged from trees (Hayssen et al., 2012). Each specimen displays little variation along the vertebral column. Wild specimens have higher and less variable TBA metrics than captive specimens, but this pattern is less visible in the direct comparisons than for *Dasypus*, *Tamandua*, and

Myrmecophaga (Figures 7d and S3; Table 3). Behaviorally, Cyclopes lies between the more active Tamandua, Myrmecophaga, and Dasypus and the slow-moving, suspensory sloths, Bradypus and Choloepus, and their TBA patterns are similarly intermediate between the clear patterns of the more active genera and the unpredictability of the sloth patterns (below). Similar research on the cortical compactness of slow arboreal mammals has found that the cortical metrics of Cyclopes resemble those of sloths due to low metabolic rate (Alfieri et al., 2020; Nagya & Montgomery, 2012).

Like captive anteaters, Bradypus and Choloepus have unpredictable bone microstructure, but potentially for different reasons. These two genera of sloths are entirely suspensory, spending their whole lives upsidedown in trees (Hayssen, 2009, 2010, 2011). Because of this lifestyle, their lumbar vertebrae are probably held in tension more than compression, unlike most other mammals. This would likely change the TBA of these vertebrae, but more specific research is needed to determine the effects of sloth posture on vertebral TBA (Røhl et al., 1991). Additionally, their slow, solitary, arboreal behavior should be fairly easy to recreate in zoos, minimizing the difference between the stresses caused in captive and wild environments (Kelleher & Ferguson, 2019; Raines, 2005). This may explain the similarities between captive and wild specimens of these genera (Figures 4e,f and S3).

Together, these findings demonstrate that the differences between captive and wild environments have impacts on TBA, and bone microstructure more generally. Because these differences are likely caused by a wide variety of factors including diet, activity level, pathology, and stereotypies, there is no simple way to account for this variation in research moving forward. The differences in bone microstructure depend on both characteristics of the animals and how they were treated in captivity during their lifetime. Therefore, caution should be exercised when using captive specimens in functional morphology research because the effects of captivity could be misinterpreted as functional signals, or the lack of functional signal where one should exist. These findings additionally imply that further progress is needed to properly recreate the habitats, diets, and behaviors of wild animals in zoos with specific focus on the very particular dietary and activity needs of Xenarthrans.

#### **ACKNOWLEDGMENTS**

We thank A. Ferguson, M. LaBarbera, Z.-X. Luo, A. Neander, J. Phelps, and C. Ross for helpful revisions and discussions of the work; access to  $\mu$ CT facilities and scanning assistance; and access to FMNH specimens and field

notes. We also thank all current and past collectors who have contributed to the FMNH mammalogy collection.

#### CONFLICT OF INTEREST

The authors declare no potential conflicts of interest.

#### **AUTHOR CONTRIBUTIONS**

Ellianna Hartrich Zack: Conceptualization (supporting); data curation (equal); formal analysis (lead); funding acquisition (equal); investigation (equal); methodology (equal); validation (equal); visualization (lead); writing - original draft (lead); writing - review and editing (equal). Stephanie Marie Smith: Conceptualization (lead); data curation (equal); formal analysis (supporting); funding acquisition (equal); investigation (supporting); methodology (supporting); resources (equal); software (equal); supervision (equal); validation (equal); writing - review and editing (equal). Kenneth David Angielczyk: Conceptualization (supporting); formal analysis (supporting); methodology (supporting); resources (equal); software (equal); supervision (equal); writing – review and editing (equal).

#### DATA AVAILABILITY STATEMENT

Grayscale and binary VOI image stacks will be made publicly available through Dryad (https://datadryad.org/stash, https://doi.org/10.5061/dryad.w3r2280rh). Full reconstructed image stacks for each specimen will be available through Morphosource (https://www.morphosource.org/, project number: 000378871) and will be deposited at the Field Museum of Natural History and linked to original specimen records through EMu.

### ORCID

Ellianna H. Zack https://orcid.org/0000-0003-4192-3488

Kenneth D. Angielczyk https://orcid.org/0000-0001-7147-2054

#### REFERENCES

- Alfieri, F., Nyakatura, J. A., & Amson, E. (2020). Evolution of bone cortical compactness in slow arboreal mammals. *Evolution* (NY), 75, 542–554. https://doi.org/10.1111/evo.14137
- Amson, E. (2019). Overall bone structure as assessed by slice-by-slice profile. *Evolutionary Biology*, *46*(4), 343–348. https://doi.org/10.1007/s11692-019-09486-6
- Amson, E., Arnold, P., van Heteren, A. H., Canoville, A., & Nyakatura, J. A. (2017). Trabecular architecture in the forelimb epiphyses of extant xenarthrans (Mammalia). *Frontiers in Zoology*, 14(1), 1–17. https://doi.org/10.1186/s12983-017-0241-x

- Amson, E., & Bibi, F. (2021). Differing effects of size and lifestyle on bone structure in mammals. *BMC Biology*, *19*(1), 1–18. https://doi.org/10.1186/s12915-021-01016-1
- Amson, E., & Nyakatura, J. A. (2018). The postcranial musculoskeletal system of xenarthrans: Insights from over two centuries of research and future directions. *Journal of Mammalian Evolution*, *25*(4), 459–484. https://doi.org/10.1007/s10914-017-9408-7
- Ancona, K. A., & Loughry, W. J. (2009). Time budgets of wild nine-banded armadillos. *Southeastern Naturalist*, 8(4), 587–598. https://doi.org/10.1656/058.008.0402
- Arenales, A., Gardiner, C. H., Miranda, F. R., Dutra, K. S., Oliveira, A. R., Mol, J. P., Texeira da Costa, M. E. L., Tinoco, H. P., Coelho, C. M., Silva, R. O., Pinto, H. A., Hoppe, E. G. L., Werther, K., & Lima Santos, R. (2020). Pathology of free-ranging and captive Brazilian anteaters. *Journal of Comparative Pathology*, 180, 55–68. https://doi.org/10.1016/j.jcpa.2020.08.007
- Armitage, P. L. (1983). Jawbone of a South American monkey from Brooks Wharf, City of London. *London Archaeologist Associa*tion. 4, 262–270.
- Barak, M. M., Lieberman, D. E., & Hublin, J. J. (2011). A Wolff in sheep's clothing: Trabecular bone adaptation in response to changes in joint loading orientation. *Bone*, 49(6), 1141–1151. https://doi.org/10.1016/j.bone.2011.08.020
- Bathke, A. C., Harrar, S. W., & Madden, L. V. (2008). How to compare small multivariate samples using nonparametric tests. *Computational Statistics and Data Analysis*, *52*(11), 4951–4965. https://doi.org/10.1016/j.csda.2008.04.006
- Canington, S. L., Sylvester, A. D., Burgess, M. L., Junno, J. A., & Ruff, C. B. (2018). Long bone diaphyseal shape follows different ontogenetic trajectories in captive and wild gorillas. *American Journal of Physical Anthropology*, 167(2), 366–376. https://doi.org/10.1002/ajpa.23636
- Clavel, J., Escarguel, G., & Merceron, G. (2015). mvMORPH: An R package for fitting multivariate evolutionary models to morphometric data. *Methods in Ecology and Evolution*, *6*(11), 1311–1319. https://doi.org/10.1111/2041-210X.12420
- Clerici, G. P., Rosa, P. S., & Costa, F. R. (2018). Description of digging behavior in armadillos *Dasypus novemcinctus* (Xenarthra: Dasypodidae). *Mastozoologia Neotropical*, 25(2), 283–291. https://doi.org/10.31687/SAREMMN.18.25.2.0.04
- Cowin, S. C. (1986). Wolff's law of trabecular architecture at remodeling equilibrium. *Journal of Biomechanical Engineering*, 108(1), 83–88. https://doi.org/10.1115/1.3138584
- Crawshaw, G. J., & Oyarzun, S. E. (1996). Vertebral hyperostosis in anteaters (*Tamandua tetradactyla* and *Tamandua mexicana*): Probable hypervitaminosis A and/or D. *Journal of Zoo and Wildlife Medicine*, 27(2), 158–169.
- Doube, M., Klosowski, M. M., Arganda-Carreras, I., Cordelières, F. P., Dougherty, R. P., Jackson, J. S., Schmid, B., Hutchinson, J. R., & Shefelbine, S. J. (2010). BoneJ: Free and extensible bone image analysis in ImageJ. *Bone*, 47(6), 1076–1079. https://doi.org/10.1016/ j.bone.2010.08.023
- Ellis, A. R., Burchett, W. W., Harrar, S. W., & Bathke, A. C. (2017). Nonparametric inference for multivariate data: The R package npmv. *Journal of Statistical Software*, 76(1), 1–18. https://doi.org/10.18637/jss.v076.i04
- Gaudin, T. J. (1999). *The morphology of xenarthrous vertebrae* (Mammalia: Xenarthra) (Vol. 41). Field Museum of Natural History. https://doi.org/10.5962/bhl.title.5269

- Gaudin, T. J., & Biewener, A. A. (1992). The functional morphology of xenarthrous vertebrae in the armadillo *Dasypus novemcinctus* (Mammalia, Xenarthra). *Journal of Morphology*, 214(1), 63–81. https://doi.org/10.1002/jmor.1052140105
- Gaudin, T. J., Hicks, P., & Di Blanco, Y. (2018). Myrmecophaga tridactyla (Pilosa: Myrmecophagidae). Mammalian Species, 50(956), 1–13. https://doi.org/10.1093/mspecies/sey001
- Gaudin, T. J., & Nyakatura, J. A. (2018). Epaxial musculature in armadillos, sloths, and opossums: Functional significance and implications for the evolution of back muscles in the Xenarthra. *Journal of Mammalian Evolution*, *25*(4), 565–572. https://doi.org/10.1007/s10914-017-9402-0
- Gibb, G. C., Condamine, F. L., Kuch, M., Enk, J., Moraes-Barros, N., Superina, M., Poinar, H. N., & Delsuc, F. (2016). Shotgun mitogenomics provides a reference phylogenetic framework and timescale for living xenarthrans. *Molecular Biology and Evolution*, 33(3), 621–642. https://doi.org/10.1093/molbev/msv250
- Guo, X. E., & Kim, C. H. (2002). Mechanical consequence of trabecular bone loss and its treatment: A three-dimensional model simulation. *Bone*, 30(2), 404–411. https://doi.org/10.1016/S8756-3282(01)00673-1
- Han, S., & Garner, M. M. (2016). Soft tissue mineralization in captive 2-toed sloths. *Veterinary Pathology*, 53(3), 659–665. https://doi.org/10.1177/0300985815598206
- Harbers, H., Zanolli, C., Cazenave, M., Theil, J. C., Ortiz, K., Blanc, B., Locatelli, Y., Schafberg, R., Lecompte, F., Baly, I., Laurens, F., Callou, C., Herrel, A., Puymerail, L., & Cucchi, T. (2020). Investigating the impact of captivity and domestication on limb bone cortical morphology: An experimental approach using a wild boar model. *Scientific Reports*, 10(1), 1–14. https:// doi.org/10.1038/s41598-020-75,496-6
- Hayssen, V. (2009). *Bradypus tridactylus* (Pilosa: Bradypodidae). *Mammalian Species*, 839, 1–9. https://doi.org/10.1644/839.1
- Hayssen, V. (2010). Bradypus variegatus (Pilosa: Bradypodidae). Mammalian Species, 42(850), 19–32. https://doi.org/10.1644/850.1
- Hayssen, V. (2011). Choloepus hoffmanni (Pilosa: Megalonychidae). Mammalian Species, 43(873), 37–55. https://doi.org/10.1644/873.1
- Hayssen, V., Miranda, F., & Pasch, B. (2012). Cyclopes didactylus (Pilosa: Cyclopedidae). Mammalian Species, 44(895), 51–58.
- Huiskes, R., Ruimerman, R., Van, L. G. H., & Janssen, J. D. (2000). Effects of mechanical forces on maintenance and adaptation of form in trabecular bone. *Nature*, 405(June), 1999–2001.
- Joo, Y. I., Sone, T., Fukunaga, M., Lim, S. G., & Onodera, S. (2003). Effects of endurance exercise on three-dimensional trabecular bone microarchitecture in young growing rats. *Bone*, 33(4), 485–493. https://doi.org/10.1016/S8756-3282(03)00212-6
- Kelleher, K. A., & Ferguson, A. (2019). Hand rearing a Linné's twotoed sloth *Choloepus didactylus* at ZSL London Zoo. *Interna*tional Zoo Yearbook, 53(1), 287–300. https://doi.org/10.1111/ izy.12235
- Ketcham, R. (2005). Three-dimensional grain fabric measurements using high-resolution X-ray computed tomography. *Journal of Structural Geology*, *27*, 1217–1228. https://doi.org/10.1016/j.jsg. 2005.02.006
- Ketcham, R., & Ryan, T. (2004). Quantification and visualization of anisotropy in trabecular bone. *Journal of Microscopy*, 213, 158–171. https://doi.org/10.1111/j.1365-2818.2004.01277.x

- King, J. D., Muhlbauer, M. C., & James, A. (2011). Radiographic diagnosis of metabolic bone disease in captive bred mountain chicken frogs (Leptodactylus fallax). Zoo Biology, 30(3), 254–259. https://doi.org/10.1002/zoo.20322
- Kivell, T. L. (2016). A review of trabecular bone functional adaptation: What have we learned from trabecular analyses in extant hominoids and what can we apply to fossils? *Journal of Anatomy*, 228(4), 569–594. https://doi.org/10.1111/joa. 12446
- Kivell, T. L., Skinner, M. M., Lazenby, R., & Hublin, J. J. (2011). Methodological considerations for analyzing trabecular architecture: An example from the primate hand. *Journal of Anatomy*, 218(2), 209–225. https://doi.org/10.1111/j.1469-7580.2010.01314.x
- Mason, G. J. (1991). Stereotypies: A critical review. Animal Behaviour, 41(6), 1015–1037. https://doi.org/10.1016/S0003-3472(05) 80640-2
- Mielke, M., Wölfer, J., Arnold, P., Van Heteren, A. H., Amson, E., & Nyakatura, J. A. (2018). Trabecular architecture in the sciuromorph femoral head: Allometry and functional adaptation. *Zoological Let*ters, 4(1), 1–11. https://doi.org/10.1186/s40851-018-0093-z
- Nagya, K. A., & Montgomery, G. G. (2012). Field metabolic rate, water flux and food consumption by free-living silky anteaters (*Cyclopes didactylus*) in Panama. *Edentata*, *13*(1), 61–65. https://doi.org/10.5537/020.013.0106
- Navarrette, D., & Ortega, J. (2010). *Tamandua mexicana* (Pilosa: Myrmecophagidae). *Mammalian Species*, 43(874), 56–63.
- Odgaard, A. (1997). Three-dimensional methods for quantification of cancellous bone architecture. *Bone*, 20(4), 315–328. https://doi.org/10.1016/S8756-3282(97)00007-0
- Oliver, J. D., Jones, K. E., Hautier, L., Loughry, W. J., & Pierce, S. E. (2016). Vertebral bending mechanics and xenarthrous morphology in the nine-banded armadillo (*Dasypus novemcinctus*). The Journal of Experimental Biology, 219(19), 2991–3002. https://doi.org/10.1242/jeb.142331
- Olson, R. A., Womble, M. D., Thomas, D. R., Glenn, Z. D., & Butcher, M. T. (2016). Functional morphology of the forelimb of the nine-banded armadillo (*Dasypus novemcinctus*): Comparative perspectives on the myology of Dasypodidae. *Journal of Mammalian Evolution*, 23(1), 49–69. https://doi.org/10.1007/s10914-015-9299-4
- O'Regan, H. J., & Kitchener, A. C. (2005). The effects of captivity on the morphology of captive, domesticated and feral mammals. *Mammal Review*, 35(35), 215–230. http://www.auburn.edu/academic/classes/biol/5090/boyd/Captivity\_effects.pdf
- Panagiotopoulou, O., Pataky, T. C., Day, M., Hensman, M. C., Hensman, S., Hutchinson, J. R., & Clemente, C. J. (2016). Foot pressure distributions during walking in African elephants (*Loxodonta africana*). *Royal Society Open Science*, *3*(10), 160203. https://doi.org/10.1098/rsos.160203
- Panagiotopoulou, O., Pataky, T. C., & Hutchinson, J. R. (2019). Foot pressure distribution in white rhinoceroses (*Ceratotherium simum*) during walking. *PeerJ*, 2019(5), 1–15. https://doi.org/10. 7717/peerj.6881
- R Core Team. (2020). R: A language and environment for statistical computing.
- Raines, J. (2005). Captive health and husbandry of the bradypodidae. *Zoo Biology*, 24(6), 557–568. https://doi.org/10. 1002/zoo.20072

- Revell, L. J. (2010). Phylogenetic signal and linear regression on species data. *Methods in Ecology and Evolution*, 1(4), 319–329. https://doi.org/10.1111/j.2041-210x.2010.00044.x
- Røhl, L., Larsen, E., Linde, F., Odgaard, A., & Jørgensen, J. (1991).
  Tensile and compressive properties of cancellous bone. *Journal of Biomechanics*, 24(12), 1143–1149. https://doi.org/10.1016/0021-9290(91)90006-9
- Rood, J. P. (1970). Notes on the behavior of the pygmy armadillo. *Journal of Mammalogy*, 51(1), 179–179. https://doi.org/10.2307/1378557
- RStudio Team. (2020). RStudio: Integrated development for R. Retrieved from http://www.rstudio.com/
- Ruff, C. B., Holt, B., & Trinkaus, E. (2006). Who's afraid of the big bad Wolff?: "Wolff's law" and bone function adaptation. American Journal of Physical Anthropology, 91(May 2007), 85–91. https://doi.org/10.1002/ajpa
- Schindelin, J., Arganda-Carreras, I., Frise, E., Kaynig, V., Longair, M., Pietzsch, T., Preibisch, S., Rueden, C., Saalfeld, S., Schmid, B., Tinevez, J. Y., White, D. J., Hartenstein, V., Eliceiri, K., Tomancak, P., & Cardona, A. (2012). Fiji: An open-source platform for biological-image analysis. *Nature Methods*, 9(7), 676–682. https://doi.org/10.1038/nmeth.2019
- Shaw, J. H., Machado-Neto, J., & Carter, T. S. (1987). Behavior of free-living giant anteaters (*Myrmecophaga tridactyla*). Biotropica, 19(3), 255–259.
- Silva, M. J., & Gibson, L. J. (1997). Modeling the mechanical behavior of vertebral trabecular bone: Effects of age-related changes in microstructure. *Bone*, *21*(2), 191–199. https://doi.org/10.1016/S8756-3282(97)00100-2
- Smith, S. M., & Angielczyk, K. D. (2020). Deciphering an extreme morphology: Bone microarchitecture of the hero shrew backbone (Soricidae: Scutisorex). *Proceedings of the Royal Society B: Biological Sciences*, 287(1926), 20200457. https://doi.org/10. 1098/rspb.2020.0457
- Sode, M., Burghardt, A. J., Nissenson, R. A., & Majumdar, S. (2008). Resolution dependence of non-metric trabecular structure indices. *Bone*, 42(4), 728–736.
- Sugiyama, T., Price, J. S., & Lanyon, L. E. (2010). Functional adaptation to mechanical loading in both cortical and cancellous bone is controlled locally and is confined to the loaded bones. *Bone*, *46*(2), 314–321. https://doi.org/10.1016/j.bone.2009.08.054

- Ulrich, D., Van Rietbergen, B., Laib, A., & Rüegsegger, P. (1999). The ability of three-dimensional structural indices to reflect mechanical aspects of trabecular bone. *Bone*, *25*(1), 55–60. https://doi.org/10.1016/S8756-3282(99)00098-8
- Vesterby, A., Gundersen, H. J. G., & Melsen, F. (1989). Star volume of marrow space and trabeculae of the first lumbar vertebra: Sampling efficiency and biological variation. *Bone*, *10*(1), 7–13. https://doi.org/10.1016/8756-3282(89)90140-3
- Vu, V., Marwick, B., Hester, J., & Held, M. (2011). ggbiplot. Retrieved from https://github.com/vqv/ggbiplot
- Wickham, H. (2016). ggplot2: Elegant graphics for data analysis.
- Wickham, H., Averick, M., Bryan, J., Chang, W., McGowan, L., François, R., Grolemund, G., Hayes, A., Henry, L., Hester, J., Kuhn, M., Pedersen, T., Miller, E., Bache, S., Müller, K., Ooms, J., Robinson, D., Seidel, D., Spinu, V., ... Yutani, H. (2019). Welcome to the Tidyverse. *Journal of Open Source Software*, 4(43), 1686. https://doi.org/10.21105/joss.01686
- Willie, B. M., Zimmermann, E. A., Vitienes, I., Main, R. P., & Komarova, S. V. (2020). Bone adaptation: Safety factors and load predictability in shaping skeletal form. *Bone*, 131(July 2019), 115114. https://doi.org/10.1016/j.bone.2019.115114
- Wolff, J. (1893). Das gesetz der traansformation der knochen. Deutsche Medizinische Wochenschrift, 19, 1222–1224.
- Zuccarelli, M. D. (2004). Research article: Comparative morphometric analysis of captive vs. wild African lion (*Panthera leo*) skulls. *Bios*, 75(4), 131–138. https://doi.org/10.1893/0005-3155(2004) 075<0131:cmaocv>2.0.co;2

#### SUPPORTING INFORMATION

Additional supporting information may be found in the online version of the article at the publisher's website.

**How to cite this article:** Zack, E. H., Smith, S. M., & Angielczyk, K. D. (2021). Effect of captivity on the vertebral bone microstructure of xenarthran mammals. *The Anatomical Record*, 1–18. <a href="https://doi.org/10.1002/ar.24817">https://doi.org/10.1002/ar.24817</a>